Identification of Optimum Cable Vibration Absorbers Using Fixed-Sized-Inerter Layouts

Jiannan Luo[1], John H.G. Macdonald[2], Jason Zheng Jiang[1]

[1] *Department of Mechanical Engineering, University of Bristol, Bristol, BS8 1TR, UK.*

[2] *Department of Civil Engineering, University of Bristol, Bristol, BS8 1TR, UK.*

Abstract

Cables are widely used in cable-stayed bridges and other civil engineering structures, but they often experience large amplitude vibrations due to their low inherent damping. Recent studies have shown that inerter-based vibration absorbers with two or three elements can provide significant performance improvements with very large inertance. Such large inertance leads to difficulties in physical implementation. Meanwhile, alternative inerter-based layouts with more elements could potentially provide better performance with significantly smaller inertance. However, studying these configurations one by one is impractical because the number of possible absorber layouts increases exponentially with the number of elements. This paper, using two types of fixed-sized-inerter (FSI) layouts, presents an efficient and systematic optimum configuration identification methodology. A simplification procedure is also adopted to then simplify the obtained configurations while not compromising the performance gains. Using this approach, it is shown that when the number of elements is increased from three to four, significant enhancement can be obtained even with small inertance values. The proposed approach can also be applied to vibration problems of other mechanical structures and with other performance criteria.

Keywords: stay cable, vibration suppression, network synthesis, damping performance, optimum configuration identification

1. Introduction

Cables are widely used in cable-stayed bridges and other civil engineering structures because of their high axial strength and stiffness. However, due to their high flexibility in the transverse direction and low intrinsic damping, cables are often observed to experience large amplitude vibrations under various excitation mechanisms. Often, the exact excitation mechanisms are unclear, but possible causes include aerodynamic forcing on the cables, such as rain-wind excitation [1, 2], galloping [3, 4], wake galloping [5], and excitation from deck or pylon motion [6, 7]. For all mechanisms, the low inherent damping of cables is a contributory factor [8]. Typically, the inherent damping ratio

of bridge cables is less than 0.1% [9] (so most past studies on enhancing the cable damping have neglected it.) Unless suppressed, these effects may cause severe vibrations, which could result in cable or connection failures due to fatigue, or damage the corrosion protection system. A commonly-used approach to suppress the vibrations of structural cables is to install a vibration absorption device. Normally, only modes with low natural frequencies are considered as they generally experience more significant vibrations than higher frequency modes [10, 11, 12, 13, 14, 15, 16].

The current guidelines on stayed cable specify the requirements of damping systems in terms of the damping ratio (or logarithmic decrement or Scruton Number, which are proportional to damping ratio) [17, 18]. Also the damping ratio affects both the amplitude of vibrations due to buffeting or vortex shedding and the critical wind speed for the onset of aero-elastic galloping and rain-wind induced vibrations [18], as well as the critical amplitude of deck vibrations to cause parametric excitation [6]. Moreover, Zuo and Jones [19] observed large amplitude vibrations of various cables due to rain-wind excitation and similar vibrations in dry conditions up to the sixth mode, whereas Acampora et al. [20] identified significant vibrations in the first five modes.

Using cross-ties to bind several cables together can increase the natural frequencies and modal masses, hence the dynamic loading and response can be reduced. However, they are undesirable aesthetically and can be difficult to access for maintenance and inspection [12].

Viscous dampers have been used in suppressing cable vibrations for many years, e.g. on the Fred Hartman Bridge in Texas, and the Erasmus Bridge in Rotterdam [12]. Viscous dampers are normally installed normal to the cable with one end fixed to the bridge deck. The achievable optimum damping ratio for a certain mode is larger if the damper is located closer to an anti-node. However, for ease of installation and maintenance, they are usually located close to the deck end of the cable, up to about 5% of the length along the cable from the end [12]. A universal curve was presented by Pacheco et al. [13] for estimating the modal damping of stay cables with a viscous damper close to one of the supports. A formula for the universal curve was analytically derived, based on approach cable modes, by Krenk [14]. Main and Jones [10] used a similar approach to investigate a wider range of cases with a viscous damper. Then, Krenk and Høgsberg [16] presented a general approach for the effect of a transverse damping force, close to the end of a cable, on the modal vibrations.

A Tuned Mass Damper (TMD) is another type of passive absorber device that has been used in practice on cables, for example on the Øresund Bridge [20]. TMDs can provide improved performance over viscous dampers for a specific mode [21]. However, they have disadvantages, such as needing a large mass located near the mid-span of the cable and having limited performance for multiple modes [22, 23].

For further performance enhancement, an inerter-based absorber device can be used. The inerter was proposed as an ideal two-terminal mechanical element with the property that the applied force is proportional to the relative acceleration between its two terminals [24]. The introduction of the inerter concept has

fundamentally enlarged the range of dynamic properties that can be realized by passive vibration absorbers. The constant of proportionality between the force and the relative acceleration is termed inertance, with dimensions of mass. Theoretical performance advantages of inerter-based suspension systems and vibration absorbers have been identified for a wide range of mechanical systems, including road vehicles [25, 26, 27], railway vehicles [28, 29, 30], aircraft landing gear systems [31, 32, 33], building structures [34, 35, 36] and bridge cables [37]. Research efforts have also been made regarding physical realizations of inerters, which can take different forms, including rack and pinion [38], ball-screw [39], hydraulic [40] and more recently introduced fluid inerters [41, 42]. Even though larger inertance can be achieved with small device mass via mechanical or hydraulic gearing, limiting required inertance values is important for practical applications. This is because physical realizations of inerters, whether via mechanical or hydraulic gearing, can only achieve a limited range of inertance in practice, for example due to weight or space constraints.

Increased attention has recently been given to suppressing cable vibrations with inerters. Lazar et al. [43] demonstrated the potential benefits of adding a Tuned Inerter Damper (TID) layout. Note that in the present study, a layout is defined as a network representing the topological connections of spring, damper and inerter elements, while a configuration refers to a layout with specific element values. More recently, Lu et al. [44] examined the damping enhancement potential of a specific absorber layout termed as viscous inerter mass damper, showing improvements of the achievable modal damping ratio, over that of a conventional viscous damper.

Shi and Zhu [45] presented an analytic solution for the dynamics of a cable with an inerter-parallel-damper layout named the inerter damper. These previous investigations on this topic have been focused on specific network layouts, although many alternatives exist. Luo et al. [46] analyzed all layouts with no more than one inerter, one damper and one spring, and identified beneficial configurations for damping ratio enhancement, considering multiple modes. It was noticed, however, that significant performance enhancement can only be achieved with large inertance. For example, it was shown that, including a constraint for higher modes, for the best three-element configuration the critical damping ratio can be improved by 451% compared with a damper only, with an inertance equal to 2.25 times the total cable mass. However, for a more realistic inertance, e.g. 50% of the cable total mass, the maximum improvement in damping ratio over a damper only reduces to 16%. Layouts with more elements give more possibility to provide greater improvements with smaller inertance. However, according to graph theory [47], as the number of elements grows, the number of possible layouts increases exponentially. Therefore, a systematic optimum configuration identification methodology is needed.

For inerter-based vibration absorber layouts with more elements, network synthesis theory, which originated in the electrical domain [48], provides a promising way forward for this systematic investigation. A fixed-sized-inerter (FSI) layout was introduced by Zhang et al. [35] for building vibration suppression, which covers a set of seven-element network layouts with one inerter and at

most six damper and spring elements. However, it will be shown in this study that no significant performance improvement for cable vibration suppression can be obtained with this FSI compared with the best three-element layout. To further expand the range of network layouts covered, another FSI layout is introduced in the present study. With these two FSI layouts, an approach for the identification of optimum cable vibration absorber configurations is introduced. It will be demonstrated that the newly-introduced FSI layout can significantly enhance the performance with small inertance values. A simplification procedure is then adopted to reduce the obtained seven-element configurations to four-element ones, which can be useful for practical implementation.

It is worth pointing out that the contributions of this work, compared with the previous publications on the same topic [43, 44, 45, 46] are the following. Firstly, a significantly wider range of inerter-based vibration absorber layouts are investigated using the two FSI layouts. Secondly, a simplification procedure is adopted to minimize the number of elements in the obtained beneficial configurations, while not compromising the performance. And thirdly, significantly enhanced damping performance with small inertance values is obtained.

This paper is organized as follows: In Section 2, a finite difference cable model with a generic vibration absorber is recalled. Two FSI absorber layouts are introduced and their respective admittance functions are derived. In Section 3, the optimum damping performance using the FSI layouts is obtained and compared with both a damper only and the best three-element absorber previously identified. In Section 4, a simplification procedure is presented, from which two four-element optimum configurations are identified, which have similar performance of the optimum FSI configurations. Conclusions are drawn in Section 5.

2. Mathematical approach

In this section, a finite difference model of a taut cable combined with an arbitrary linear passive absorber layout, established in [46], is recalled. Two different optimization measures are proposed. Then, using network synthesis, two fixed-sized-inerter layouts are introduced.

The cable vibration problem can be formulated in partial derivative form for the cable, along with additional equation(s) for the absorber. In principle this is exact, but it leads to a transcendental equation for the eigenvalues. Although asymptotic solutions for the absorber very close to the end of the cable have been found [10, 13, 16], the form of the equation is different for each different absorber layout so there is not a general analytically solution. Furthermore, it is necessary to use approximate or numerical solutions, at which point the benefit of the exact equation of motion for the cable is somewhat lost. The proposed finite difference form, with the absorber represented by a generic admittance function, has the benefits of the form of the matrix equation being the same for any absorber layout and a simple, consistent method can be used for its solution for the eigenvalues. By discretising the cable into a sufficiently large number of lumped masses, this formulation converges on the exact solution.

2.1. Cable model with integrated absorber admittance function

A mathematical model of a taut cable combined with a linear absorber layout was built in [46], using the finite difference method, and is reviewed briefly here. Neglecting cable inclination, sag, out-of-plane motion and elasticity of the cable, a lumped finite difference model with n degrees of freedom (DOFs) is built, with a general absorber represented by an admittance function $Y(s)$ at one location, as shown in Figure 1. The tension along the cable is denoted T, the total mass of the cable is M and the total length of the cable is L. The circular natural frequency of Mode 1 of the undamped cable is $\omega_0 = \pi(T/ML)^{0.5}$. There are n masses, each of mass m spread along the cable and two masses of mass $m/2$ connected directly to the supports. Hence, $m = M/(n+1)$. These masses divide the cable into $n+1$ elements, each of length l equal to $L/(n+1)$. In this paper n is taken to be 99, as this was previously shown to give an appropriate balance of accuracy and computing time [46]. The a^{th} mass has an associated transverse displacement $x_a(t)$, which equals zero at equilibrium. The absorber is connected to mass a_f. Since the masses at the end-points are connected directly to the supports, which are assumed to be fixed, x_0 and x_{n+1} are always equal zero.

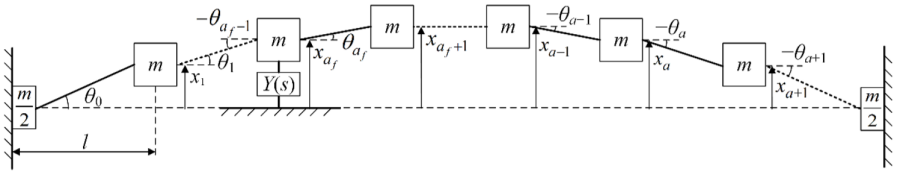

Figure 1: Finite difference model of a taut cable with an absorber with admittance function$Y(s)$.

Considering Figure 1, the equation of motion of each mass can be derived. Then, by taking Laplace transforms of both sides, the following equation for each mass is obtained [46],

$$\frac{1}{n+1}s^2\widetilde{x}_a = (n+1)\cdot(\frac{\omega_o}{\pi})^2\cdot(\widetilde{x}_{a-1} - 2\widetilde{x}_a + \widetilde{x}_{a+1}) + \delta_{aa_f}\frac{Y(s)}{M}\cdot s\cdot\widetilde{x}_{a_f}(s) \quad (1)$$

where δ_{aa_f} represents the Kronecker delta function, the tildes indicate Laplace transforms and $Y(s) = \widetilde{F}(s)/[s\cdot\widetilde{x}_{a_f}(s)]$ represents the admittance function of the absorber, which is defined as the ratio of force to relative velocity of its terminals. It has been shown that all admittance functions representing linear, passive absorbers are positive-real functions [49]. By arranging the displacement of each mass in the vector $\widetilde{\mathbf{x}} = [\widetilde{x}_1, \widetilde{x}_2, \widetilde{x}_3, \cdots, \widetilde{x}_n]^{\mathrm{T}}$, Equation (1) can be rewritten in matrix form as

$$\mathbf{M}s^2\widetilde{\mathbf{x}} + \mathbf{C}s\widetilde{\mathbf{x}} + \mathbf{K}\widetilde{\mathbf{x}} = 0 \quad (2)$$

in which $\mathbf{M}$, $\mathbf{C}$ and $\mathbf{K}$ are the mass, damping and stiffness matrices respectively. The inherent damping of the cable is neglected in line with previous studies

[10, 11, 12, 13, 14, 15, 21, 22, 43, 44, 45], so all elements of the damping matrix are zero except for the one representing the absorber. The elements of $\mathbf{M}$, $\mathbf{C}$ and $\mathbf{K}$ are respectively defined as

$$m_{ij} = \frac{1}{n+1}\delta_{ij}$$

$$c_{ij} = 0, \text{ except } c_{afaf} = -Y(s)/M$$

$$k_{ij} = (n+1)\cdot(\frac{\omega_o}{\pi})^2 \cdot (2\delta_{ij} - \delta_{i(j+1)} - \delta_{i(j-1)})$$

The complex eigenvalues of the system, represented by $[\boldsymbol{\lambda} \quad \boldsymbol{\lambda}^{*\mathrm{T}}]^{\mathrm{T}}$,(where superscript* indicates the complex conjugate) can be calculated as the roots of

$$\det\left(\begin{bmatrix} \mathbf{0} & \mathbf{I} \\ -\mathbf{M}^{-1}\mathbf{K} & -\mathbf{M}^{-1}\mathbf{C} \end{bmatrix} - \lambda \begin{bmatrix} \mathbf{I} & \mathbf{0} \\ \mathbf{0} & \mathbf{I} \end{bmatrix}\right) = 0 \tag{3}$$

where det means the determinant, $\boldsymbol{\lambda} = [\lambda_1, \lambda_2, \lambda_3, \cdots]$, $\mathbf{0}$ is the square null matrix of size n and $\mathbf{I}$ is the identity matrix of size n.

Hence, the eigenvalue of Mode i (i.e., λ_i) of the damped cable can be obtained. Accordingly, the damping ratio ζ_i and circular natural frequency ω_i of Mode i can be calculated, respectively as

$$\zeta_i = -\mathrm{Re}(\lambda_i)/\sqrt{\mathrm{Re}(\lambda_i)^2 + \mathrm{Im}(\lambda_i)^2} \tag{4}$$

$$\omega_i = \sqrt{\mathrm{Re}(\lambda_i)^2 + \mathrm{Im}(\lambda_i)^2} \tag{5}$$

2.2. Two performance measures

Two different measures are proposed for the optimization in this study. Measure 1 aims to maximize the damping ratio of any modes with natural frequencies close to that of the first undamped mode of the cable, while ensuring the damping ratio of the next few modes are no lower than those for a viscous damper optimized for Mode 1. This is the same performance measure as previously used for multiple modes [46]. Normally, the lowest frequency mode (i.e. Mode 1) is the most susceptible to vibrations [11]. To cover this mode and any additional mode with a similar natural frequency, introduced by the absorber, the optimization is applied to the minimum damping ratio of all modes with natural frequencies $\omega_i \in (0, 1.5\omega_0)$. Considering the damping of the rest few modes, the reference damping ratios for the cable with a viscous damper are taken from the universal curve [13]. All modes in the frequency range $\omega_i \in (1.5\omega_0, 6.5\omega_0)$ are included to ensure that the first six modes of the undamped cable are covered. Therefore, the first measure is to maximize the minimum damping ratio, defined as the critical damping ratio (denoted ζ_c) of all modes with frequencies in the range $\omega_i \in (0, 1.5\omega_0)$, with the constraint that modes with natural frequencies in the range $\omega_i \in (1.5\omega_0, 6.5\omega_0)$ have no less damping than those for a cable with a viscous damper optimized for Mode 1.

Measure 2 is to maximize the minimum η_i, over all modes of interest where η_i is defined as the product $\zeta_i \cdot \omega_i$. This measure is applicable to galloping-type aerodynamic instabilities, for which the motion of the cable in the wind causes changes in the aerodynamic forces which are equivalent to negative damping [3]. Based on quasi-steady theory, the aerodynamic damping ratio of mode i is given by [4],

$$\zeta_{ai} = \frac{\rho DUL}{4M\omega_i}\beta \tag{6}$$

where ρ is the density of air, D is the cable diameter, U is the mean wind speed and β is a function of the cable orientation and the static aerodynamic force coefficients of the cross-section. If β is negative, structural damping of at least $-\zeta_{ai}$ is required to prevent galloping, i.e. dynamic instability of the cable. Since ρ, D, U, L, M and β are all independent of the mode number, galloping of mode i occurs if the product $\eta_i = \zeta_i \cdot \omega_i$ is less than a certain value. Hence the minimum value of η_i for all modes of interest determines the threshold at which galloping would occur. For this measure, all modes in the frequency range $\omega_i \in (0, 6.5\omega_0)$ are included to ensure that the first six modes of the undamped cable are covered. Therefore, the second measure is to maximize the minimum η_i, denoted as η_c, of all modes with frequencies in the range $\omega_i \in (0, 6.5\omega_0)$.

2.3. Network synthesis and Fixed-sized-inerter layouts

It has been shown in the previous study [46] that with small inertance, only limited performance advantages compared with a damper can be achieved with absorber configurations consisting of at most one spring, one damper and one inerter. In this sub-section, two fixed-sized-inerter (FSI) layouts are introduced which include one inerter b and two sub-networks with admittance functions $S_1(s)$ and $S_2(s)$ respectively. FSI-I, shown in Figure 2(a), was defined in [35], where its benefits for vibration suppression were demonstrated for multi-story buildings. A new FSI layout, FSI-II, shown in Figure 2(b), is introduced in this paper, covering a different set of network layouts.

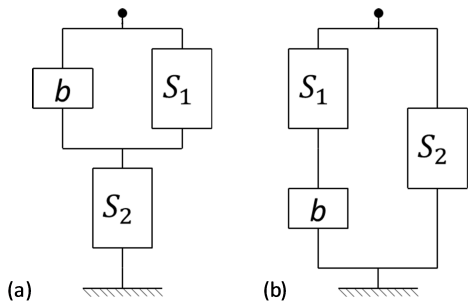

Figure 2: The two FSI layouts. (a) FSI-I and (b) FSI-II.

The admittance functions of FSI-I and FSI-II, $Y_1(s)$ and $Y_2(s)$ respectively can be derived as

$$Y_1(s) = \frac{S_2(s)[bs + S_1(s)]}{bs + S_1(s) + S_2(s)}, \tag{7a}$$

$$Y_2(s) = \frac{bsS_1(s)}{bs + S_1(s)} + S_2(s). \tag{7b}$$

The two functions, $S_1(s)$ and $S_2(s)$ are restricted to be bi-linear admittance functions, of the forms

$$S_1(s) = \frac{\alpha_1 s + \beta_1}{s + \gamma_1}, \tag{8a}$$

$$S_2(s) = \frac{\alpha_2 s + \beta_2}{s + \gamma_2}. \tag{8b}$$

To guarantee that $S_1(s)$ and $S_2(s)$ can be realized with dampers and springs only, the following two conditions need to be satisfied, according to network synthesis theory [24],

$$\alpha_1\gamma_1 - \beta_1 \leq 0, \tag{9a}$$

$$\alpha_2\gamma_2 - \beta_2 \leq 0. \tag{9b}$$

These two FSI layouts cover a wide range of candidate network layouts for investigation and also fully control the inertance b, so as to facilitate the identification of beneficial absorber configurations with practical inertance values.

3. Optimum performance of FSI layouts

For generality, the inertance is non-dimensionlized using the total weight of the cable, i.e., letting $b' = b/M$. Similarly, the circular natural frequencies of the damped system and the distance of the damper from one end, relative to the total cable length are also presented in non-dimensional form as $\omega_i{}' = \omega_i/\omega_0$ and $a'_f = a_f/(n+1)$ respectively. A value of $a'_f = 0.05$ is chosen as an example for the investigation in the present study. It is worth pointing out that the approach demonstrated in this work is directly applicable to problems with other a'_f values.

In this section, for a given non-dimensional inertance b', ranging from 0 to 1, all the other parameter values in $S_1(s)$ and $S_2(s)$ are optimized according to each measure introduced in Section 2.2. The optimum results of the two FSI absorber layouts are obtained and analyzed. Matlab is used for the optimization, using the optimization function "patternsearch" to obtain approximate optimum solutions, with the genetic algorithm "GPS basis 2N" [50]. The solutions of "patternsearch" are then used as initial estimates for the gradient-based function "fminsearch" for fine-tuning. The convergence criterion for both "patternsearch" and "fminsearch" is a certain pre-determined tolerance on the

change in the value of the cost function over the iteration. In this study, the relative tolerance is set to be 1×10^{-4}. Furthermore, to identify the global minimum, multiple starting points are used for the "patternsearch" optimization.

3.1. Optimum results for Measure 1

Based on the established cable model, the optimum critical damping ratio, denoted as $\zeta_{c,opt}$, can be obtained for Measure 1. In Figure 3, the dashed curve represents the optimum results for FSI-I, and the solid curve for FSI-II. Results for layouts with fewer elements are also shown in Figure 3 for comparison. The dotted curve is the optimum performance that can be achieved by all three-element layouts previously considered [46], and the cross shows the optimized damping ratio of Mode 1 for a viscous damper only, with a value of 0.026. It can be seen that both FSI layouts can provide greater optimum critical damping ratio than that for three-element layouts. Compared with FSI-I, FSI-II is more beneficial as it provides better optimum critical damping ratio for all inertance values considered. It should be noted in particular that, with non-dimensional inertance $b' < 0.36$, the benefits of FSI-II grow rapidly with increasing b'.

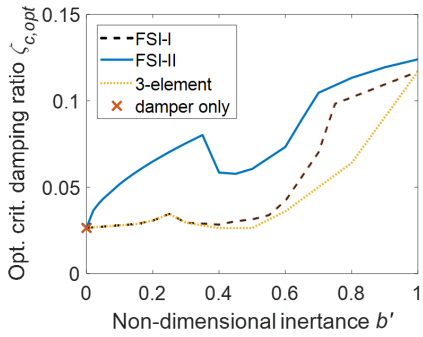

Figure 3: Optimum critical damping ratio (Measure 1) versus non-dimensional inertance for layouts FSI-I, FSI-II, three-element layout and damper only.

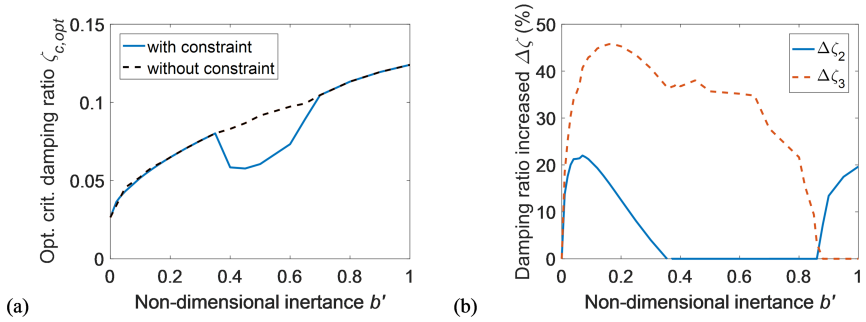

Figure 4: Influence of the higher mode constraint of Measure 1 for FSI-II. (a) Optimum critical damping ratio versus non-dimensional inertance with and without constraint, (b) percentage increase in damping ratios of Modes 2 and 3 with the constraint over a damper only optimized for Mode 1.

The influence of the higher mode constraint on the optimization results of Layout FSI-II is presented in Figure 4. The optimum results with and without the constraint are compared in Figure 4(a). For non-dimensional inertance $0.36 < b' < 0.7$, the optimum critical damping ratio is significantly influenced by the constraint, but for other inertance values the difference between the optimized results with and without the constraint is minimal.

The percentage increases in the damping ratios of Modes 2 and 3, for FSI-II with the higher mode constraint over a damper only, optimized for Mode 1, are presented in Figure 4(b). When non-dimensional inertance $b' < 0.36$, the optimized results are not influenced by the higher-mode constraint. For $0.36 < b' < 0.86$ the optimized results are limited by Mode 2. For $b' > 0.86$ the optimized results are limited by Mode 3, though for $b' > 0.70$ the difference in the results with and without the constraint is negligible. Modes 4 to 6 are not shown in the figure as they do not influence the results.

3.2. Optimum results for Measure 2

The optimization results for the two FSI layouts against Measure 2, i.e., the optimum critical η_c (denoted as $\eta_{c,opt}$), are presented in Figure 5(a), which shows the relationship between $\eta_{c,opt}$ and non-dimensional inertance b', with a dashed curve for FSI-I and a solid curve for FSI-II. The cross shows the performance of a viscous damper only for comparison.

It can be seen from Figure 5(a) that for most values of b' considered, FSI-II provides much greater $\eta_{c,opt}$ than FSI-I. For both FSI-1 and FSI-II with $b' = 0$, $\eta_{c,opt} = 0.026$, which is the same as for a viscous damper only. Compared with the $\eta_{c,opt} = 0.063$ for $b' = 1$, the local optimum value $\eta_{c,opt} = 0.055$ for a small inertance of $b' = 0.09$ is only marginally less effective, and it provides a 112% of increase in the value compared with a damper only.

Figure 5(b) presents η_i for the first two modes for the optimized solutions for FSI-II in Figure 5(a). When the non-dimensional inertance $b' < 0.09$, the limiting value is given by η_1, while for $0.09 < b' < 1$, the limiting value is provided by η_2. The values of η_i of higher modes are not limiting, so they are not shown in Figure 5(b).

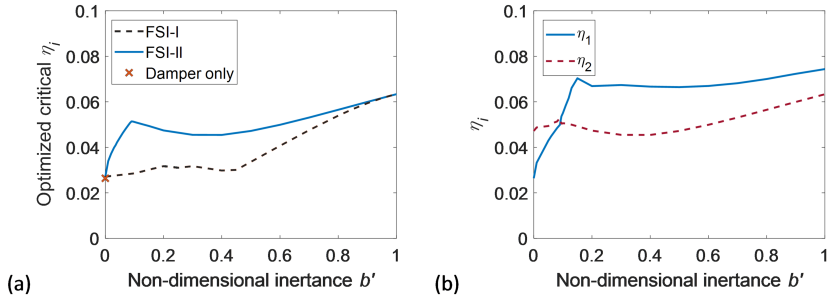

Figure 5: $\eta_{c,opt}$ versus non-dimensional inertance. (a) Optimum results for layouts FSI-I, FSI-II and damper only, (b) η_i for Modes 1 and 2 for the optimized FSI-II.

4. Optimum performance with simplified configurations

In the previous section, significant advantages against both performance measures have been identified for the FSI-II layout (illustrated in Figure 2(b)) with small inertance values. However, to realize these identified configurations, networks with seven elements are required. For example, using the Foster preamble [48] one of the possible mechanical structures of FSI-II is shown in Figure 6. For physical implementation of a mechanical vibration absorber, it is highly desirable to minimize the number of elements, so in this section a simplification procedure is carried out. The optimum performance of the simplified configurations is then compared with that of the optimized results for FSI-II. The values of the damping coefficient and stiffness of the dampers and springs are expressed in non-dimensional form as $c'_j = (c_j/M)/\omega_0$ and $k'_j = (k_j/M)/(\omega_0)^2$, where c_j and k_j are the physical damping coefficient and stiffness, respectively.

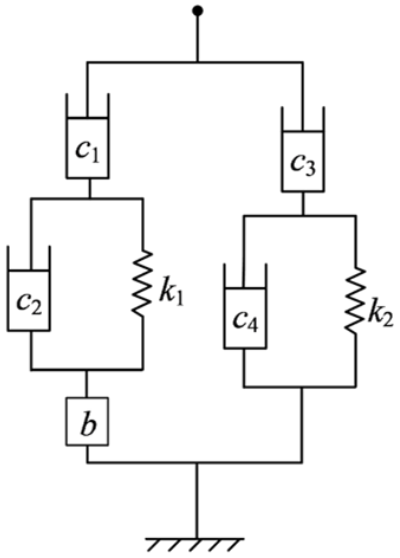

Figure 6: One possible mechanical structure of FSI-II.

4.1. Simplification approach

The simplification procedure is carried out in the following way. The optimization in Section 3 for FSI-II finds multiple local maximum of the critical damping ratio (Measure 1) or critical η_i (Measure 2) with very similar results but for different values of the parameters in Equations (8a) and (8b). It was found that for some results, γ_1 in $S_1(s)$ is very small, and for other results, α_1 in $S_1(s)$ is very small. If γ_1 or α_1 is set to zero, $S_1(s)$, which in general can be realized by the sub-network shown in Figure 7(a), can then be realized by the layouts shown in Figures 7(b) or 7(c), correspondingly.

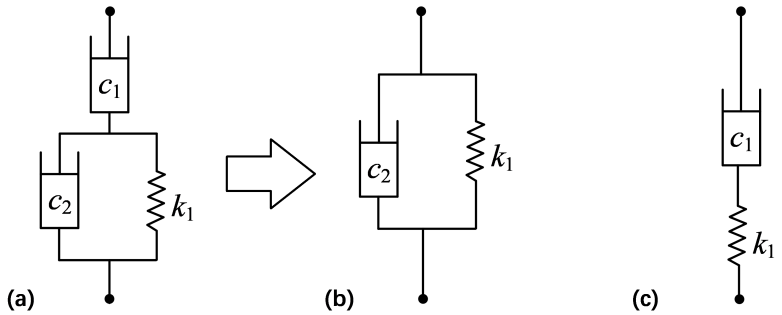

Figure 7: S_1 and its simplifications. (a) One of the possible sub-networks realizing S_1 (Equation 8(a)) in FSI-II, (b) S_1 simplified to a spring-parallel-damper layout for $\gamma_1 = 0$, and (c) S_1 simplified to a spring-series-damper layout for $\alpha_1 = 0$.

Similarly, it was found that for all of the optimized results, the values of α_2, β_2 and γ_2 in Equation (8b) make $S_2(s)$ close to a constant value. If $S_2(s)$, which in general can be realized by the sub-network in Figure 8(a), is simplified to a constant, then it can be realized by a damper only, shown in Figure 8(b). Hence the seven-element layout of Figure 6 (or alternative equivalent layouts) is simplified to a four-element layout. Depending on whether S_1 is simplified to Figures 7(b) or 7(c), two different four-element layouts, L_A and L_B shown in Figures 9(a) and 9(b), are obtained. It is important to note that, whether the admittance function for FSI-II, given by Equation (7b), is realized by the mechanical structure in Figure 6 or one of the alternative equivalent structures, the simplifications that γ_1 or α_1 equals zero and $S_2(s)$ is a constant lead to the same two simplified structures L_A and L_B in Figure 9.

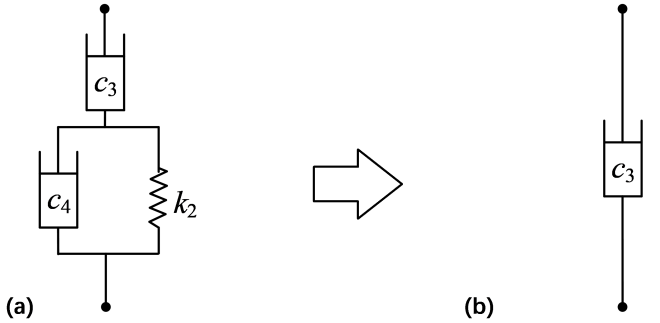

Figure 8: S_2 and its simplification. (a) One of the possible sub-networks realizing $S_2(s)$ (Equation (8b)) in FSI-II, and (b) sub-networks S_2 simplified to a damper only when its admittance $S_2(s)$ is set to a constant.

The values of the performance measures for the simplified layouts are compared with the optimum values achieved for FSI-II in Section 3, which can be realized by the seven-element network shown in Figure 6. Where difference in the performance values is less than 1%, the simplification is considered fully justified. It is worth pointing out that, after the above simplification procedure, even though the parameter values of the remaining elements in Figure 9 are very close to those for the global minimum, an optimization is still carried out for fine tuning to obtain more accurate results.

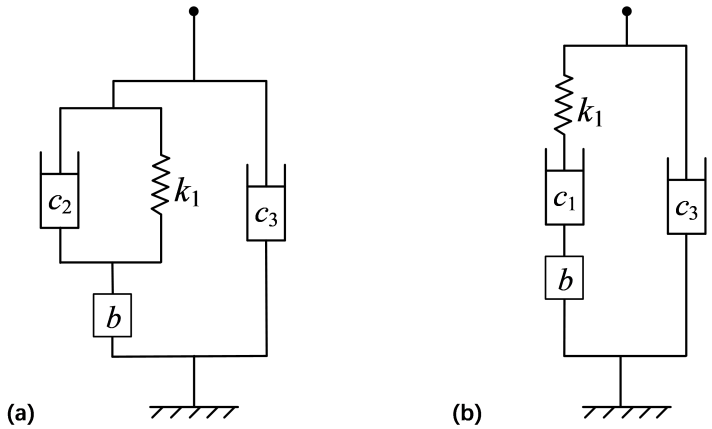

Figure 9: Mechanical structures of simplified four-element layouts. (a) Simplified layout L_A and (b) simplified layout L_B.

4.2. Performance for Measure 1

For Measure 1, the optimum critical damping ratio $\zeta_{c,opt}$ for Layouts L_A and L_B are compared with results for FSI-II and a damper only in Figure 10(a). The corresponding non-dimensional damping coefficients c_1', c_2', c_3' and spring stiffness k_1' are respectively shown in Figures 10(b), 10(c) and 10(d).

It can be seen from Figure 10(a) that the optimum critical damping ratio $\zeta_{c,opt}$ provided by the simplified layout L_A is virtually the same as that for FSI-II, which requires seven elements to realize, for the full range of b' considered, while L_B is similarly effective only for $b' \leq 0.36$. Figures 10(c) and 10(d) show that for $b' \leq 0.36$ both layouts require virtually the same values of c_3' and k_1'. For both simplified layouts, the value of $\zeta_{c,opt}$ is not affected by the higher mode constraint for $b' \leq 0.36$. Figure 10(b) shows that c_2' in L_A requires a lower damping coefficient than c_1' in L_B. It should be noted that although for L_A, c_2' is very small for $b' < 0.2$, it cannot be removed as there is then a significant loss in optimum damping ratio.

In Figure 10(d), an approximately linear relationship can be found between the non-dimensional inertance b' and the corresponding non-dimensional spring stiffness k_1' for $b' < 0.9$ for L_A and $b' \leq 0.4$ for L_B. This can be explained as follows. The frequency provided by the ratio k_1'/b' is approximately equal to one, i.e., the natural frequency of the inerter-spring sub-system is close to that of the first undamped mode of the cable. Hence, b' and k_1' are essential to Mode 1 of the cable. Previous results have shown that for a three-element layout without the parallel damper [46], very beneficial damping ratios can be achieved for Mode 1 of the cable, but when the higher mode constraint is applied the benefit is marginal. For the four-element layout proposed here, c_3' is smaller than the value of damping coefficient for the damper only optimized for Mode 1 as shown in Figure 10(c). However, combining c_3' with the tuned

spring-inerter-damper sub-system, the two types of four-element layouts lead to most beneficial damping ratio enhancement for Mode 1, while not violating the higher mode constraint.

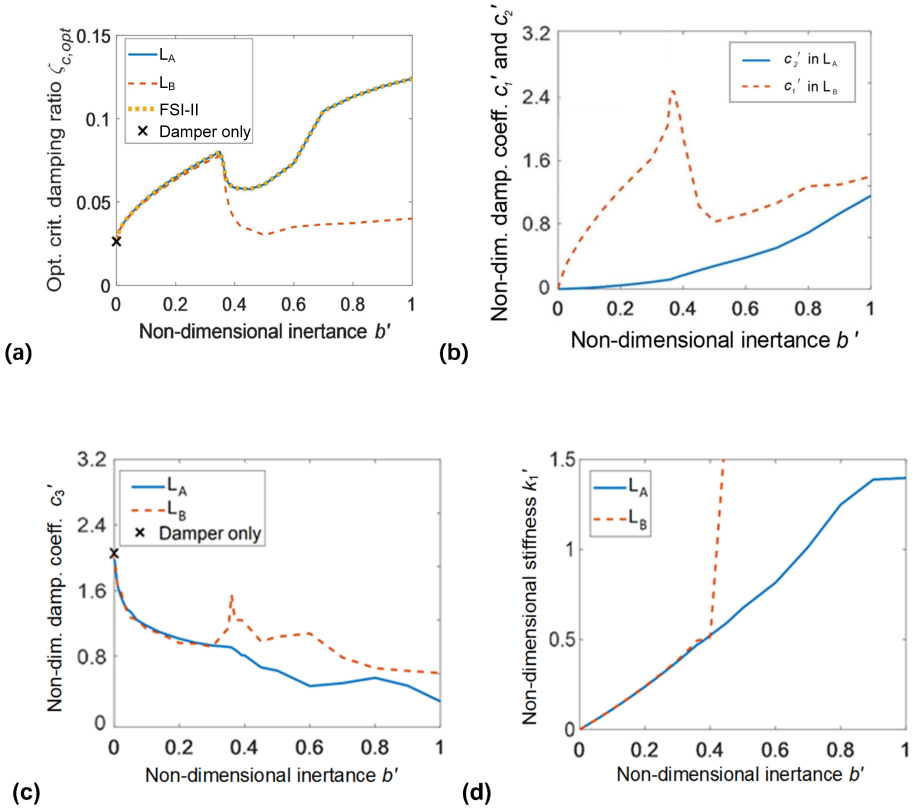

Figure 10: Optimum results for Layouts L_A and L_B for Measure 1 versus non-dimensional inertance. (a) Optimum critical damping ratio, (b) corresponding non-dimensional damping coefficients c_1' and c_2', (c) corresponding non-dimensional damping coefficient c_3' and (d) corresponding non-dimensional spring stiffness k_1'.

Taking two non-dimensionlized inertance values, b' equal to 0.05 and 0.36 as examples, the increase in damping ratio for each mode relative to a viscous damper only optimized for Mode 1, are shown in Figure 11, for L_A, L_B, as well as the optimum that can be achieved by three-element layouts [46]. It should be noted that there are two modes with same damping ratio and very similar frequencies for both L_A and L_B around $\omega_1' = 1$, due to the extra DOF(s) introduced by the absorber layouts. Otherwise the changes to the natural frequencies due to the addition of the absorber are small.(Changes in natural frequencies due to the addition of absorbers are discussed in mire detail in the previous

paper [46]).

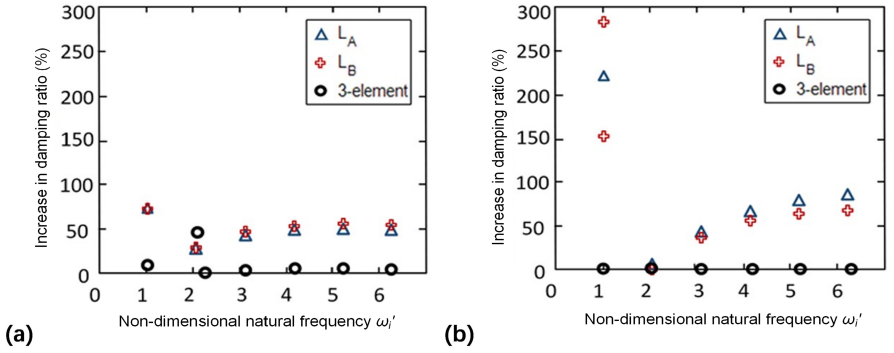

Figure 11: Increases in damping ratio for each mode relative to an optimized viscous damper for Mode 1 for Measure 1. (a) For non-dimensional inertance b' of 0.05, and (b) for b' of 0.36.

It can be seen from Figure 11 that, for the two example values of non-dimensional inertance considered, the performance advantages of optimum three-element layout are marginal, which is consistent with the conclusion in [46]. In comparison, significant enhancements are observed for both L_A and L_B. Comparing the two simplified beneficial layouts, L_A provides the greater relative improvements for $b' = 0.36$, while with $b' = 0.05$, both layouts give very similar results for Mode 1 and L_B is slightly better for the higher modes. With non-dimensional inertance b' of 0.05 shown in Figure 11(a), the relative improvement of Layout L_A over a viscous damper is 72% for Mode 1, which corresponding to 63% improvement compared with the most beneficial three-element layout. The damping ratios of the higher modes are also larger than the optimum damper only case. Thus, the higher mode constraint does not affect the results. This is because with L_A tuned to its maximum performance for Mode 1 it also has beneficial effects on the higher modes. For $b' = 0.36$, as none of the three-element layouts provides any benefits compared with a damper only, the corresponding points in Figure 11(b) are all on the 0% increase line. It can also be calculated that the optimum critical damping ratio $\zeta_{c,opt}$ for L_A for Mode 1 is 206% of both the viscous damper only case and the most beneficial three-element layout. It can also be seen form Figure 11(b) that the critical mode has the frequency close to the second mode's frequency of a damper only. For $b' > 0.36$, the constraint on Mode 2 causes a reduction on the achievable optimum critical damping ratio as observed in Figure 10(a).

4.3. Performance for Measure 2

For Measure 2, $\eta_{c,opt}$(optimal critical η_i) for L_A, L_B and the optimized seven-element FSI-II are presented and compared in Figure 12 along with the corresponding element values. As shown in Figure 12(a), L_A provides almost

the same performance as FSI-II over the whole range of studied inertance, but L_B can only achieve this with $b' \leq 0.25$. It can be seen from Figures 12(b) and 12(c) that L_A requires the same or a lower damping coefficient for c_3' and a lower coefficient for the other damper (c_1' and c_2') than L_B. Also, the required parallel damping c_3' for both L_A and L_B are much less than that of an optimum damper alone. Figure 12(d) shows that, in the range of $b' < 0.7$ for L_A and $b' < 0.5$ for L_B, the non-dimensional stiffness k_1' increases with b' almost proportionally. It can be calculated that the internal resonance of the absorber is close to the cable's first mode. For L_B with $b' \geq 0.5$, k_1' tends to be infinity, indicating that a optimum of L_B is three-element layout with two dampers and one inerter only, which leads to is less beneficial performance compared with the original FSI-II and the simplified L_A.

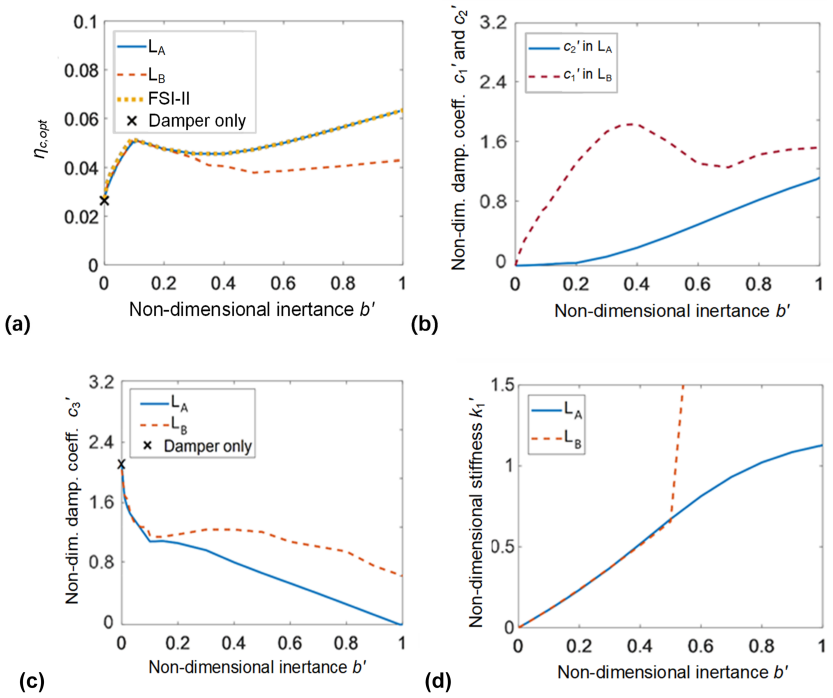

Figure 12: Optimum results for Layouts L_A and L_B for Measure 2 versus non-dimensional inertance. (a) $\eta_{c,opt}$, (b) corresponding non-dimensional damping coefficients c_1' and c_2', (c) corresponding non-dimensional damping coefficient c_3' and (d) corresponding non-dimensional spring stiffness k_1'.

For the inertance provides the local maximum for Measure 2, i.e. $b' = 0.09$, the corresponding η_i for all modes within the natural frequency range of 0 to $6.5\omega_0$ are presented in Figure 13, for L_A and L_B and the most beneficial three-

element layout identified in [46]. It can be seen that all the absorber layouts have minor influence on the cable's natural frequencies. It can also be seen that three-element layouts can only provide marginal improvements compared with the damper only case. On the other hand, an improvement of around 102% for $\eta_{c,opt}$ is achieved for both L_A and L_B. This corresponds to around 84% improvement compared with the most beneficial three-element layout. It worth to point out that because of the additional degrees of freedom introduced by L_A and L_B are tuned for Mode 1, there are two close modes around $\omega_1' = 1$ in Figure 13 for both the L_A and L_B cases, with very similar values of η_i.

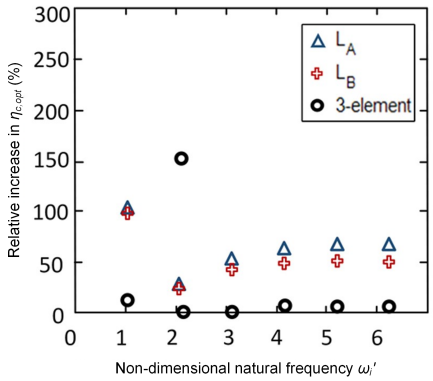

Figure 13: Relative increase in corresponding η_i for all modes in natural frequency range of 0 to $6.5\omega_0$ for b' of 0.09.

5. Conclusion

In this paper, with a finite difference model of the cable-absorber system and two proposed performance measures, an investigation has been carried out to identify absorber layouts that have substantially better performance with low inertance values, compared with both a viscous damper only and previously studied three-element layouts. The systematic identification is facilitated by two fixed-sized-inerter (FSI) layouts generated via network synthesis. The FSI layouts cover a subset of all 7-element layouts with inerters, dampers and springs, and have the advantage of being able to fix or constraint the inertance value. The results show that both FSI layouts can provide enhanced performance, while Layout FSI-II can provide significantly better damping performance for all inertance values investigated. Following a simplification procedure, two four-element layouts L_A and L_B are identified. It worth to be noted that when the problem setup is changed (e.g. with different absorber layouts, performance measures number), the network layouts will probably be different (i.e. with different element number and/or different topological connections). The results indicate that for low inertance values, both simplified layouts can provide very similar performance, while Layout L_A is as effective as FSI-II over a wider range

of inertance and meanwhile requires a lower damping coefficient for one of the dampers. Taking a non-dimensional inertance value of 0.05 and the first measure as an example, both L_A and L_B can achieve 72% and 63% improvements compared with the optimum damper and the most beneficial three-element layouts, respectively. The level of improvement with low inertance values is critical for future real-life implementation. The promising results obtained demonstrate the significant potential of the network-synthesis-based approach to cover wider ranges of candidate absorber layouts.The approach established in this study can work with the existing guidelines [12, 18, 17] to design inerter-based vibration absorbers for cables on cable-staged bridges, and also it can be directly applicable to other vibration suppression problems.

6. Acknowledgements

Mr Jiannan Luo is funded by the China Scholarship Council for his PhD study and Dr Jason Zheng Jiang is supported by EPSRC Grant EP/P013456/1.

References

[1] Y. Hikami, N. Shiraishi, Rain-wind induced vibrations of cables in cable-stayed bridges, Journal of Wind Engineering and Industrial Aerodynamics 29 (1988) 409–418.

[2] M. Matsumoto, N. Shiraishi, M. Kitazawa, C. Knisely, H. Shirato, K. Y., M. Tsujii, Aerodynamic behaviour of inclined circular cylinders-cable aerodynamics, Journal of Wind Engineering and Industrial Aerodynamics 33(1-2) (1990) 63–72.

[3] J. P. Den Hartog, Transmission line vibration due to sleet, Transactions of the American Institute of Electrical Engineers 51(4) (1933) 1074–1076.

[4] J. H. G. Macdonald, G. L. Larose, A unified approach to aerodynamic damping and drag/lift instabilities, and its application to dry inclined cable galloping, Journal of Fluids and Structures 22(2) (2006) 229–252.

[5] S. Tokoroa, H. Komatsub, M. Nakasub, K. Mizuguchic, A. Kasugad, A study on wake-galloping employing full aeroelastic twin cable model, Journal of Wind Engineering and Industrial Aerodynamics 88 (2000) 247–261.

[6] J. L. Lilien, A. P. Da Costa, Vibration amplitudes caused by parametric excitation of cable stayed structures, Journal of Sound and Vibration 174(1) (1994) 69–90.

[7] J. H. G. Macdonald, Multi-modal vibration amplitudes of taut inclined cables due to direct and/or parametric excitation, Journal of Sound and Vibration 363 (2016) 473–494.

[8] J. H. G. Macdonald, Separation of the contributions of aerodynamic and structural damping in vibrations of inclined cables, Journal of Wind Engineering and Industrial Aerodynamics 90(1) (2002) 19–39.

[9] H. Yamaguchi, Y. Fujino, Stayed cable dynamics and its vibration control, Symposium on Advances in Bridge Aerodynamics (1998) 235253.

[10] J. A. Main, N. P. Jones, Free vibrations of taut cable with attached damper. I: Linear viscous damper, Journal of Engineering Mechanics 128(10) (2002) 1062–1071.

[11] N. J. Gimsing, C. T. Georgakis, Cable supported bridges: concept and design (3rd edition), Wiley & Sons, London, UK, 2011.

[12] E. Caetano, Cable vibrations in cable-stayed bridges, Int. Association for Bridge and Structural Engineering, Zurich, Switzerland, 2007.

[13] B. M. Pacheco, Y. Fujino, A. Sulekh, Estimation curve for modal damping in stay cables with viscous damper, Journal of Structural Engineering 119(6) (1993) 1961–1979.

[14] S. Krenk, Vibrations of a taut cable with an external damper, Journal of Applied Mechanics 67(4) (2000) 772–776.

[15] S. Krenk, J. Høgsberg, Tuned resonant mass or inerter-based absorbers: unified calibration with quasi-dynamic flexibility and inertia correction, Proceedings of the Royal Society A 472(2185) (2016) 20150718.

[16] S. Krenk, J. R. S. Høgsberg, Damping of cables by a transverse force, Journal of Engineering Mechanics 131(4) (2005) 340–348.

[17] SETRA, Cable Stays: Recommendations of French Inter ministerial Commission on Prestressing, Center des Techniques des Ouvraes dArt, Bagneux Cedex, France., 2002.

[18] PTI, Recommendations for Stay-Cable Design, Testing, and Installation, Post Tensioning Institute, PTI DC45.1-12, Farmington Hills, MI, USA., 2012.

[19] D. Zuo, N. Jones, Interpretation of field observations of wind-and rain-wind-induced stay cable vibrations, Journal of Wind Engineering and Industrial Aerodynamics 98 (2010) 7387.

[20] A. Acampora, J. H. G. Macdonald, T. Georgakisa, N. Nikitas, Identification of aeroelastic forces and static drag coefficients of a twin cable bridge stay from full-scale ambient vibration measurements, Journal of Wind Engineering and Industrial Aerodynamics 124: (2014) 90–98.

[21] K. N. Bakis, M. Massaro, M. S. Williams, J. Graham, Passive control of bridge wind-induced instabilities by tuned mass dampers and movable flaps, Journal of Engineering Mechanics 143(9) (2017) 04017078.

[22] C. S. Cai, W. Wu, X. M. Shi, Cable vibration reduction with a hung-on tmd system. part I: Theoretical study, Journal of Vibration and Control 12(7) (2006) 801–814.

[23] V. H. Cu, B. Han, A stay cable with viscous damper and tuned mass damper, Australian Journal of Structural Engineering 16(4) (2015) 316–323.

[24] M. C. Smith, Synthesis of mechanical networks: The inerter, IEEE Transactions on Automatic Control 47(10) (2002) 1648–1662.

[25] M. C. Smith, F. C. Wang, Performance benefits in passive vehicle suspensions employing inerters, Vehicle System Dynamics 42(4) (2004) 235–257.

[26] J. Z. Jiang, X. Liu, A. Harrison, Passive suspension incorporating inerters for road damage improvement of heavy vehicles, Symposium on Dynamics

of Vehicles on Road and Tracks (2015) Graz, Austria.

[27] Y. Shen, L. Chen, X. Yang, D. Shi, J. Yang, Improved design of dynamic vibration absorber by using the inerter and its application in vehicle suspension, Journal of Sound and Vibration 361 (2016) 148–158.

[28] F. C. Wang, M. K. Liao, B. H. Liao, W. J. Su, H. A. Chan, The performance improvements of train suspension systems with mechanical networks employing inerters, Vehicle System Dynamics 47(7) (2009) 805–830.

[29] F. C. Wang, M. R. Hsieh, H. J. Chen, Stability and performance analysis of a full-train system with inerters, Vehicle System Dynamics 50(4) (2012) 545–571.

[30] J. Z. Jiang, A. Z. Matamoros-Sanchez, A. Zolotas, R. M. Goodall, M. C. Smith, Passive suspensions for ride quality improvement of two-axle railway vehicles, Proceedings of Institution of Mechanical Engineers (Part F): Journal of Rail and Rapid Transit 229(3) (2015) 315–329.

[31] Y. Liu, M. Z. Q. Chen, Y. Tian, Nonlinearities in landing gear model incorporating inerter, IEEE International Conference on Information and Automation (2015) 696–701.

[32] Y. Li, C. Howcroft, J. Z. Jiang, S. A. Neild, Using continuation analysis to identify shimmy-suppression devices for an aircraft main landing gear, Journal of Sound and Vibration 408(10) (2017) 234–251.

[33] Y. Li, J. Z. Jiang, S. A. Neild, Inerter-based configurations for main landing gear shimmy suppression, Journal of Aircraft 54(2) (2017) 684–693.

[34] N. Makris, G. Kampas, Seismic protection of structures with supplemental rotational inertia, Journal of Engineering Mechanics 142(11) (2016) 04016089.

[35] Y. Zhang, J. Z. Jiang, S. A. Neild, Optimal configurations for a linear vibration suppression device in a multi-storey building, Structural Control and Health Monitoring 24(3) (2017) e1887.

[36] M. Wang, F. Sun, Displacement reduction effect and simplified evaluation method for sdof systems using a clutching inerter damper, Earthquake Engineering and Structural Dynamics 47(7) (2018) 1651–1672.

[37] I. F. Lazar, S. A. Neild, D. J. Wagg, Vibration suppression of cables using tuned inerter dampers, Engineering Structures 122(1) (2016) 62–71.

[38] M. Lazarek, P. Brzeski, P. Perlikowski, Design and identification of parameters of tuned mass damper with inerter which enables changes of inertance, Mechanism and Machine Theory 119 (2018) 161–173.

[39] C. Papageorgiou, M. C. Smith, Laboratory experimental testing of inerters, 44th IEEE Conference on Decision and Control, and the European Control Conference (2005) Seville, Spain.

[40] F. C. Wang, M. F. Hong, T. C. Lin, Designing and testing a hydraulic inerter, Journal of Mechanical Engineering Science 225(1) (2011) 66–72.

[41] S. J. Swift, M. C. Smith, A. R. Glover, C. Papageorgiou, B. Gartner, N. Houghton, Design and modelling of a fluid inerter, International Journal of Control 86(11) (2013) 2035–2051.

[42] X. Liu, J. Z. Jiang, B. Titurus, A. Harrison, Model identification method-

ology for fluid-based inerters, Mechanical Systems and Signal Processing 106 (2018) 479–494.

[43] I. F. Lazar, S. A. Neild, D. J. Wagg, Using an inerterbased device for structural vibration suppression, Earthquake Engineering & Structural Dynamics 43(8) (2014) 1129–1147.

[44] L. Lu, Y. F. Duan, B. F. Spencer, X. Lu, Y. Zhou, Inertial mass damper for mitigating cable vibration, Structure Control and Health Monitoring 24(10) (2017) e1986.

[45] X. Shi, S. Zhu, Dynamic characteristics of stay cables with inerter dampers, Journal of Sound and Vibration 423 (2018) 287–305.

[46] J. Luo, J. Z. Jiang, J. Macdonald, Cable vibration suppression with inerter-based absorbers, Journal of Engineering Mechanics 145(2) (2019) 04018134.

[47] J. Riordan, C. E. Shannon, The number of two-terminal series-parallel networks, Studies in Applied Mathematics 21(1-4) (1942) 83–93.

[48] M. Van Valkenburg, Introduction to modern network synthesis, John Wiley & Sons, New York, USA, 2007.

[49] O. Brune, Synthesis of a finite two-terminal network whose driving-point impedance is a prescribed function of frequency, Studies in Applied Mathematics 10(1-4) (1931) 191–236.

[50] R. M. Lewis, V. Torczon, Pattern search algorithms for bound constrained minimization, SIAM Journal on Optimization 9(4) (1999) 1082–1099.